Journal of ELECTRONIC MATERIALS, Vol. 40, No. 9, 2011
DOI: 10.1007/s11664-011-1681-2

Enhancement of the Stability of Ti and Ni Ohmic Contacts to 4H-SiC with a Stable Protective Coating for Harsh Environment Applications

WALTER DAVES,[1,4] ANDREAS KRAUSS,[1] VOLKER HÄUBLEIN,[2] ANTON J. BAUER,[2] and LOTHAR FREY[2,3]

1.—Robert Bosch GmbH, Robert-Bosch-Platz 1, 70839 Gerlingen, Germany. 2.—Fraunhofer IISB, Schottkystrasse 10, 91058 Erlangen, Germany. 3.—University of Erlangen–Nuremberg, Chair of Electron Devices, Cauerstrasse 6, 91058 Erlangen, Germany. 4.—e-mail: walter.daves@de.bosch.com

We report on wafer-level measurements of the long-term stability of Ti and Ni ohmic contacts to *n*-4H-SiC during thermal treatments in air or air/moisture environments up to 500°C. Contact metallizations with and without a sputtered Ti (20 nm)/$TaSi_x$ (200 nm)/Pt (150 nm) diffusion barrier stack and Ti (20 nm)/TiN (10 nm)/Pt (150 nm)/Ti (20 nm) interconnects were compared. A protective coating consisting of a SiO_x (250 nm)/SiN_y (250 nm) stack deposited by plasma-enhanced chemical vapor deposition (PECVD) was used. The stability of the contact metallizations during long-term thermal treatments in air and air/moisture was studied. The best performance was achieved with Ti ohmic contacts without the Ti/$TaSi_x$/Pt stack. This system successfully withstood 1000 h thermal treatment at 500°C in air followed by 1000 h at 500°C in air/10% moisture. After the aging, the contact failure ratio was below 1% and the specific contact resistivity amounted to $(2.5 \pm 1.1) \times 10^{-4}\ \Omega\ cm^2$. Scanning electron microscopy (SEM) cross-sectional analysis indicated no degradation in the contact metallization, demonstrating the effectiveness of the SiO_x/SiN_y protective coating in preventing oxidation of the contacts. These results are very promising for applications in harsh environments, where the stability of ohmic contacts is crucial.

Key words: 4H-SiC, ohmic contact, protective coating, reliability, harsh environment

INTRODUCTION

Efforts to increase energy efficiency and reduce greenhouse-gas emissions demand robust sensor and electronic devices operating in harsh environments. The most common application scenarios are found in the automotive, aerospace, and avionics industries.[1] Silicon carbide (SiC) is a promising material for harsh environment sensors and electronics due to its outstanding properties and the high level of maturity of the related process technology.[2] The lifetime of SiC devices in harsh environments is above all limited by the stability of the contact metallization, the interconnects, and the device packaging. In combustion and exhaust gas environments, especially due to the presence of moisture up to 10% concentration, the oxidation resistance of ohmic contacts is a major concern. In the presence of moisture or impurities such as Na or Cl, oxidation dynamics in particular is largely enhanced.[3,4] Okojie et al. reported outstanding results regarding the long-term stability of Ti contacts to 4H-SiC and 6H-SiC at high temperatures in air, achieving a figure of merit of 1000 h at 600°C.[5,6] In that work, a tantalum silicide ($TaSi_x$) layer was employed as a diffusion barrier between the Ti contact and the Pt top layer. The most critical reaction mechanisms were identified, consisting on the one hand in oxidation of the PtSi overlayer

(Received February 18, 2011; accepted May 23, 2011; published online June 21, 2011)

formed after the decomposition of the $TaSi_x$ layer and on the other hand in TiSi formation in the interface zone.[7] Other works on $TaSi_x$ thin films employed as a diffusion barrier for ohmic contacts to SiC reported poor oxidation resistance for this material at temperatures at and above 500°C in air.[8,9] In those works, the lifetime of $TaSi_x$/Pt and Ni/$TaSi_x$/Pt contact metallizations at 500°C in air was limited to ~200 h by the oxidation of the $TaSi_x$ layer. In Ref. 9, a better oxidation resistance was achieved with TiW/Ti/Pt contacts. However, the oxidation resistance still remains challenging, since stability at high temperatures in air/moisture environment is required for the applications mentioned above.

In this work we propose, therefore, a different approach to achieve the required stability. This approach consists of the deposition of a stable protective coating on the contact metallization, thus preventing incorporation of oxygen into the contact region. We demonstrate that this approach allows achievement of the desired stability with comparably simple contact metallization stacks, implementing a protective coating based on a plasma-enhanced chemical vapor deposition (PECVD) SiO_x/SiN_y stack on Ti and Ni-based contact metallizations to *n*-4H-SiC. Besides the beneficial effect on the stability of the ohmic contacts, a stable protective coating is highly desirable for sensors and electronics exposed to harsh environments, since it can inhibit degradation occurring in other device components such as active areas, interconnects or gate metallizations.[10–13]

EXPERIMENTAL PROCEDURES

We used 3-inch, Si-face, 4° off-axis 4H-SiC wafers (Cree, Inc.). The *n*-substrates (0.022 Ω cm) had a 0.5-μm-thick *n*-epilayer with a doping level of 1×10^{18} cm^{-3} and a 5-μm epilayer with a doping level of 2×10^{19} cm^{-3} on top. The wafers were coated with a 300-nm SiO_2 layer deposited by low-pressure chemical vapor deposition (LPCVD) using tetramethyl orthosilicate (TEOS) as a precursor. This layer was then annealed for 30 min at 900°C in nitrogen atmosphere and patterned by means of standard photolithography and inductively coupled plasma (ICP) etching to expose the contact areas. Then, photolithography with an image reversal resist was performed, and the wafers were cleaned in Caro's acid and dipped in HF. Immediately thereafter, the wafers were loaded into the evaporation chamber for deposition of the Ni or Ti contact metals by e-beam evaporation. After carrying out the lift-off of the resist, the contact metals were annealed for 2 min at 1100°C in Ar using a rapid thermal annealing (RTA) system. The additional metal layers were deposited onto the alloyed contacts in a sputtering chamber. These layers were sputtered subsequently without breaking the vacuum and patterned through lift-off. Samples with a Ti (20 nm)/$TaSi_x$ (200 nm)/Pt (150 nm) diffusion barrier stack and Ti (20 nm)/TiN (10 nm)/Pt (150 nm)/Ti (20 nm) interconnect on top as well as samples without the Ti/$TaSi_x$/Pt diffusion barrier stack were fabricated (Fig. 1). The final 20-nm Ti layer deposited on the Ti/TiN/Pt interconnect improved the adhesion of the protective coating. The passivation consisted of a SiO_x (250 nm)/SiN_y (250 nm) stack and was deposited by PECVD. Finally, the contact pads were exposed by means of a photolithographic mask and ICP etching. The process parameters of wafers A to D are summarized in Table I. More details on the protective coating and the interconnects can be found in Ref. 14.

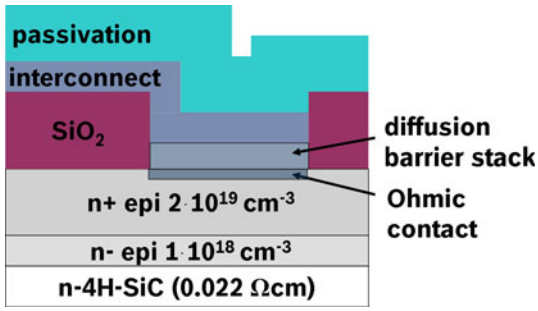

Fig. 1. Schematic cross-section of the investigated contact metallizations. Samples with a Ti (20 nm)/$TaSi_x$ (200 nm)/Pt (150 nm) diffusion barrier stack deposited onto the contacts after the annealing at 1100°C were compared with samples without the Ti/$TaSi_x$/Pt stack. The interconnects consisted in both cases of a Ti (20 nm)/TiN (10 nm)/Pt (150 nm)/Ti (20 nm) stack.

We employed a modified version of Reeves' circular transmission line method (cTLM) to determine the specific contact resistance (SCR) of the contact metallizations. The schematic layout of the contact structures is shown in Fig. 2. The structures consisted of two concentric contact rings with a varying gap of 20 μm, 30 μm, 40 μm, 50 μm, 60 μm, and 100 μm, respectively. A top view of a single cTLM structure is shown in Fig. 3a. Following Reeves, the resistance between two concentric ring contacts on a semiconductor layer reads[15,16]

$$R = R_{sh}/2\pi \cdot \ln(r_3/r_2) + R_{c1} + R_{c2}, \quad (1)$$

where R_{sh} is the sheet resistance of the semiconductor, and R_{c1} and R_{c2} are the contact resistance for the inner and the outer ring, respectively. With the specific contact resistance ρ_c and the sheet resistance of the semiconductor layer under the contacts R_{sk} we define the parameter α as $(R_{sk}/\rho_c)^{1/2}$. With the modified Bessel functions of the *n*th kind $I_n(x)$ and $K_n(x)$, the contributions of the contact resistance R_{c1} and R_{c2} can be written as[17]:

$$R_{c1} = R_{sk}/(2\pi\alpha r_2) \cdot (I_1(\alpha r_1)K_0(\alpha r_2) + I_0(\alpha r_2)K_1(\alpha r_1))/ (I_1(\alpha r_2)K_1(\alpha r_1) - I_1(\alpha r_1)K_1(\alpha r_2)); \quad (2)$$

$$R_{c2} = R_{sk}/(2\pi\alpha r_3) \cdot (I_1(\alpha r_4)K_0(\alpha r_3) + I_0(\alpha r_3)K_1(\alpha r_4))/ (I_1(\alpha r_4)K_1(\alpha r_3) - I_1(\alpha r_3)K_1(\alpha r_4)); \quad (3)$$

Table I. Fabrication process details for the investigated contact metallizations

Wafer	Doping (cm^{-3})	Contact (nm)	RTA Anneal	Diffusion Barrier Stack (nm)	Interconnect (nm)	Passivation (nm)
A	2×10^{19}	Ti 30	2 min 1100°C	$Ti/TaSi_x/Pt$ 50/200/70	Ti/TiN/Pt/Ti 20/10/150/20	SiO_x/SiN_y 250/250
B	2×10^{19}	Ni 50	2 min 1100°C	$Ti/TaSi_x/Pt$ 20/200/70	Ti/TiN/Pt/Ti 20/10/150/20	SiO_x/SiN_y 250/250
C	2×10^{19}	Ti 30	2 min 1100°C	–	Ti/TiN/Pt/Ti 20/10/150/20	SiO_x/SiN_y 250/250
D	2×10^{19}	Ni 50	2 min 1100°C	–	Ti/TiN/Pt/Ti 20/10/150/20	SiO_x/SiN_y 250/250

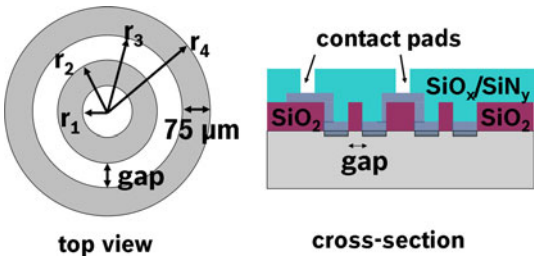

Fig. 2. Schematic layout of the employed cTLM structures consisting of two concentric rings; the gap between the rings amounted to 20 μm, 30 μm, 40 μm, 50 μm, 60 μm, and 100 μm, respectively.

We calculated the specific contact resistivity ρ_c through weighted nonlinear regression of the experimental data to Eq. (1) performed with MATHEMATICA. We used α and R_{sh} as the fitting parameters and assumed that R_{sh} was equal to R_{sk}. We note that the contributions to the total resistance given by the multilayer contact stacks and by the interconnects are neglected in this calculation. The latter assumption is fairly justified when Pt interconnects are used, since the resistivity of Pt (10.4 $\mu\Omega$ cm) is smaller than that of the silicide and carbide phases that are typically formed after the annealing of Ti or Ni contacts ($TiSi_2$, TiC, and Ni_2Si, respectively) by a factor of 2 to 3.[18] Nevertheless, the parameter ρ_c extracted with our method overestimates the actual specific semiconductor–alloy contact resistivity. We emphasize that this study did not target exact determination of ρ_c. Rather, we aimed at investigation of the stability of the total contact resistance upon thermal treatment in air and air/moisture.

The electrical measurements were carried out using a fully automatic shielded Cascade probe station. The *I–V* characteristics were measured in four-point probe configuration in the current range from −1 mA to 1 mA. A Keithley 6221 current source and a Keithley 2181A nanovoltmeter were used in the measurement. The resistance between the contacts was calculated through least-squares fitting of the measured *I–V* characteristic. The contacts were considered to be ohmic if the condition $R^2 > 0.999$ was satisfied, where R^2 is the reduced chi-squared associated to the fitting. This condition is satisfied for characteristics with good linearity. An average over all ohmic contacts was then carried out before fitting the dataset to Eq. (1). For each sample type, 126 modified cTLM structures were measured, corresponding to a total number of 1512 contact rings. The thermal treatment was performed in a furnace at 500°C with slow heating/cooling ramps of 5°C min^{-1}. The wafers were cumulatively aged up to 2000 h at 500°C, and measurements were carried out at room temperature after each aging step. Hereby, the atmosphere was switched from synthetic air (20% O_2 in N_2, total flux 1 slm) to an air/moisture mixture (10% H_2O, 10% O_2 in N_2, total flux 1 slm) after the first 1000 h. To investigate the microstructural changes induced by the aging, we carried out scanning electron microscopy (SEM) analysis and SEM cross-sectional analysis. Sample cross-sections were prepared by focused ion beam (FIB) technique using a Carl Zeiss CrossBeam 1540 system. A Pt layer with a thickness of 1 μm was deposited locally on the sample before cutting the cross-section. Cross-sections with 10 μm width and about 3 μm depth were thus prepared.

RESULTS AND DISCUSSION

Measurement of the Specific Contact Resistivity (SCR)

The SiO_x/SiN_y passivation showed good adhesion on all wafers except for the samples with a Ni contact and the $Ti/TaSi_x/Pt$ stack (wafer B). Here, partial adhesion failure occurred already during the processing (Fig. 3). This is believed to be caused by a combination of stress build-up in the $Ti/TaSi_x/Pt$ stack and in the SiO_x/SiN_y passivation, and poor adhesion properties of the Ni contact layer to the SiC semiconductor. It is known that the morphological stability of Ni contacts is limited by the segregation of C atoms and the void formation at the SiC/contact interface that occur during the silicidation reaction.[18–21] Incidentally, no adhesion failure was visible for either Ni contacts without the $Ti/TaSi_x/Pt$ stack (wafer D) or Ti contacts with the $Ti/TaSi_x/Pt$ stack (wafer A) after the processing. The magnitude of adhesion failure because of stress build-up in the $Ti/TaSi_x/Pt$ stack in wafer A is believed to be limited by the strong adhesion of Ti on SiC.

The SCR data calculated after the method described previously are summarized in Table II. The SCR of as-processed samples was generally in the range of 1.1×10^{-4} Ω cm^2 to 1.2×10^{-4} Ω cm^2, and the sheet resistance of the *n*-epilayer R_{sh}

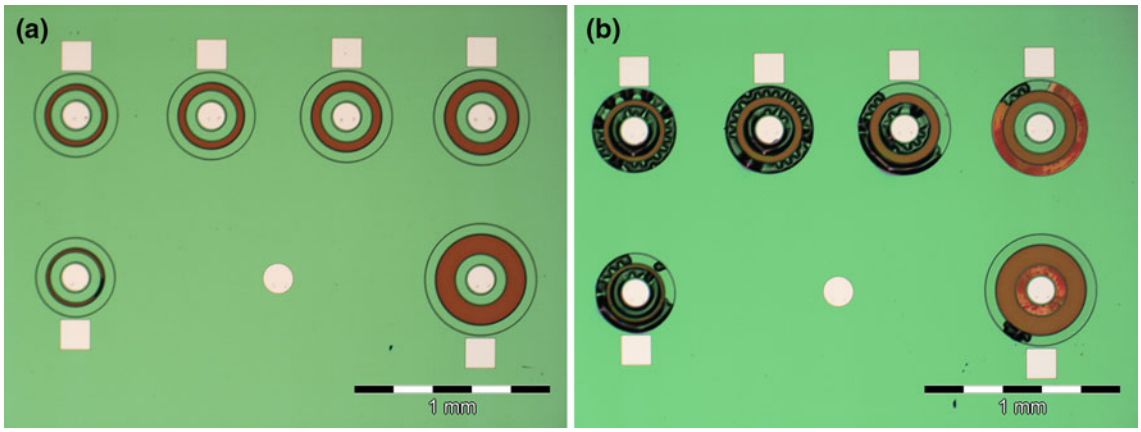

Fig. 3. Micrographs of cTLM structures in the as-processed state for Ti (a) and Ni (b) contacts with the Ti/TaSi$_x$/Pt diffusion barrier stack.

Table II. Comparison between the specific contact resistivity (SCR) in the as-processed state and after 2000 h at 500°C

Wafer	SCR New (10^{-4} Ω cm^2)	SCR after 2000 h at 500°C (10^{-4} Ω cm^2)	Failed Contacts after 2000 h at 500°C (%)
A	1.2 ± 0.4	5.3 ± 5.1	1.9
B	1.1 ± 1.1	$>10^6$	85.8
C	1.2 ± 0.5	2.5 ± 1.1	0.8
D	1.2 ± 0.4	3.0 ± 1.2	0.1

amounted to 1.5 Ω/sq (Table II). The measured SCR is larger than the best values reported in the literature for Ni and Ti contacts, which are in the range of 0.1×10^{-5} Ω cm^2 to 1×10^{-5} Ω cm^2 for n-epilayers with similar doping level.[22,23] This can be explained considering the contributions to the SCR given by the Ti/TaSi$_x$Pt diffusion barrier stack and/or the Ti/TiN/Pt interconnect, which add to the contact resistance and are not ruled out in our calculation of the SCR. For samples A, C, and D, the wafer-level statistics in the as-processed state was fairly narrow (Table II). On wafer B, the spread was larger and approximately 8% of the contacts exhibited non-ohmic characteristics. This was due to the partial adhesion failure observed already in the as-processed state (Fig. 3). The current–voltage characteristics between single contacts from wafer A in the as-processed state are shown in Fig. 4. As can be seen, the contacts have good linearity (R^2 = 1).

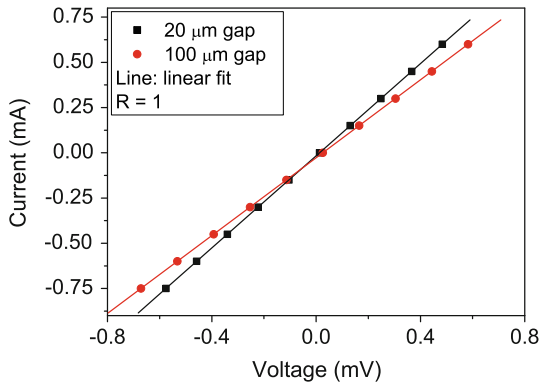

Fig. 4. Current–voltage characteristics of single Ti contacts without the Ti/TaSi$_x$/Pt stack (wafer C) in the as-processed state.

Cumulative Aging at 500°C in Air and Air/Moisture Environment

The results of the cumulative aging for wafers A, B, C, and D up to 2000 h at 500°C are summarized in Fig. 5. For wafers A, C, and D the SCR stabilized at a value of about 1.9×10^{-4} Ω cm^2 after 100 h at 500°C in air. This may be due to intermetallic reactions in the contact metallizations which increase the effective SCR value, such as the formation of PtTi phases. This mechanism was observed in a previous study on Ti/TiN/Pt/Ti interconnects passivated by a SiO$_x$/SiN$_y$ stack.[14] For wafers A, C, and D the statistical spread did not increase substantially during the first 1000 h of aging at 500°C in air (Fig. 5a, c, d). After the switch to air/moisture environment, an increase of the statistical spread and a further increase of the SCR were observed for all wafers. The SCR then stabilized again for wafers C and D, whereas for wafer A the SCR showed a slight drift towards an end value of ~5.3×10^{-4} Ω cm^2 and a further increase of the spread (Table II). For Ni contacts with the Ti/TaSi$_x$/

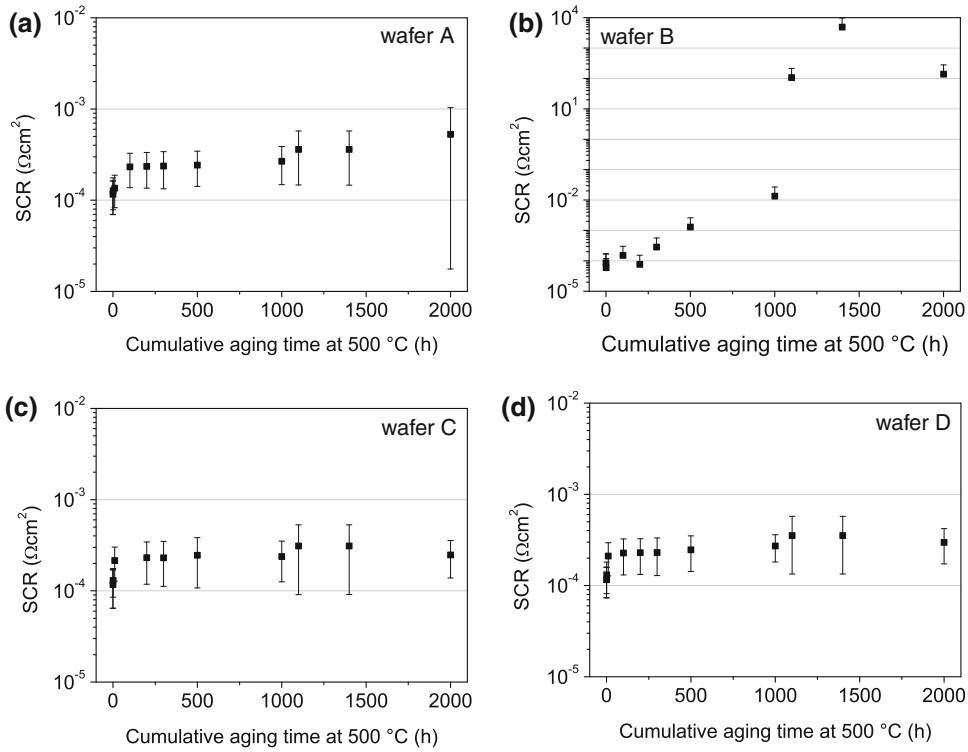

Fig. 5. Average specific contact resistance (SCR) as a function of cumulative aging time. The environment was switched from synthetic air (0.2 slm O_2/0.8 slm N_2) to air/10% moisture after the first 1000 h.

Pt diffusion barrier stack (wafer B), a very large statistical spread was present already for new samples. This was explained by the poor adhesion observed already for new samples (Fig. 3). The statistical spread increased greatly during the aging, while the fraction of the contacts preserving the ohmic character decreased. After switching to air/moisture environment, massive degradation of the SCR was visible (Fig. 5b). This resulted in spread of the order of 280 Ω cm^2 for the SCR of the ohmic contacts after 2000 h at 500°C. In Fig. 6, a comparison between the *I–V* characteristics of two single contacts from wafer B in the as-processed state and after 100 h at 500°C is shown. As can be seen, the characteristic was ohmic in the as-processed state and became diode-like after 100 h at 500°C. This contact was considered as failed according to the above-mentioned criterion ($R^2 > 0.999$). The failure statistics for wafer B as a function of aging time is shown in Fig. 7. The failure rate appears to saturate after 300 h at 500°C in air, but increases quickly after switching the environment from air to moisture/air. This indicates that oxidation plays a dominant role in the degradation of the contacts. For wafers A, C, and D, failure of less than 1% of the contacts was observed after 2000 h at 500°C. In a previous work on the Ti/TiN/Pt interconnects and the SiO_x/SiN_y passivation, we demonstrated through x-ray photoelectron spectroscopy (XPS) depth profiling that the protective coating inhibits oxidation of the Ti/TiN underlayers during thermal

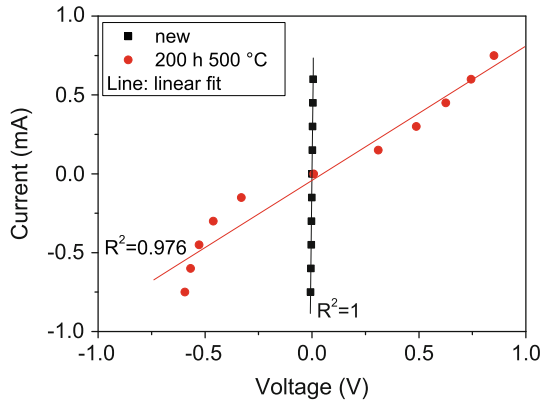

Fig. 6. Comparison between the current–voltage characteristics of a single Ni contact with the Ti/$TaSi_x$/Pt stack (wafer B) in the as-processed state and after 200 h at 500°C in air.

treatment in air at 600°C. We argue therefore that the excellent stability observed for the contact metallization in C and D is achieved because the migration of oxygen towards the contact layer is efficiently inhibited by the protective coating.

SEM Analysis and SEM Cross-Sectional Analysis of the Samples

The samples were investigated by light microscopy, SEM, and SEM cross-sectional analysis. For Ti contacts with the Ti/$TaSi_x$/Pt diffusion barrier stack (wafer A), increasing delamination of the

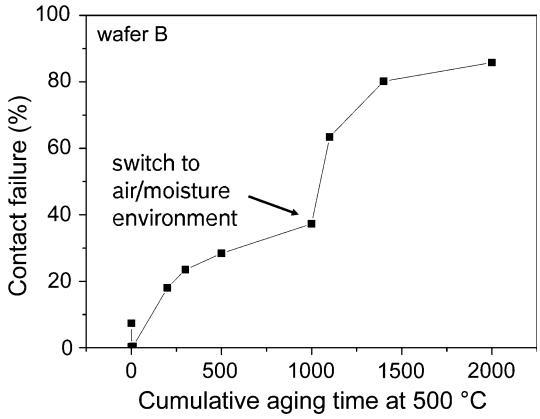

Fig. 7. Failure statistics of Ni contacts with the Ti/TaSi$_x$/Pt stack (wafer B) during cumulative aging at 500°C. The contacts were considered nonohmic if the reduced chi-squared R^2 associated to a linear regression of the *I–V* characteristics was smaller than 0.999.

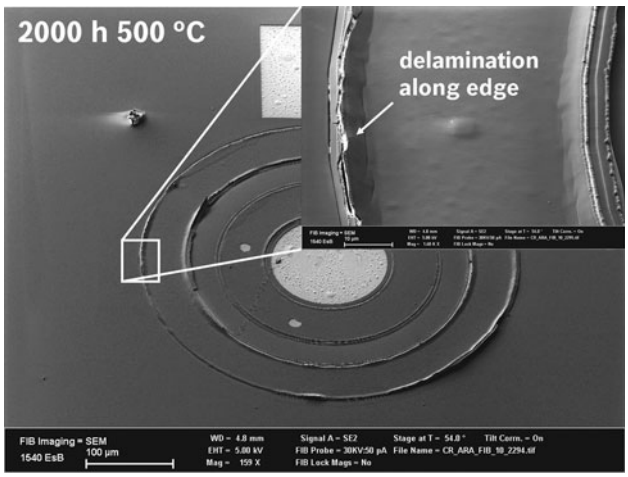

Fig. 8. Tilted SEM micrograph on a Ti contact with the Ti/TaSi$_x$/Pt stack (wafer A) after aging for 2000 h at 500°C.

contact metallization along its edges was visible during the aging. This was confirmed by the SEM analysis of samples after 2000 h at 500°C (Fig. 8). Stress build-up in the Ti/TaSi$_x$/Pt stack is probably the mechanism responsible for the delamination. As can be seen in Fig. 8, the peeling off of the contact metallization along the edges of the contact ring caused a fracture in the SiO$_x$/SiN$_y$ passivation layer. Therefore, a fraction of the contact metallization was left unprotected during part of the aging. This degradation mechanism is consistent with the large increase of the statistical spread in the SCR data that was observed for wafer A, especially after switching the environment from air to air/moisture (Fig. 5). A cross-section of the as-deposited contact metallization of wafer A before the deposition of the passivation stack is shown in Fig. 9a. In the as-deposited contact metallization, a clear material contrast is visible in the in-lens detector between the Pt and the TaSi$_x$ layer. This contrast corresponds to the higher conductivity of the Pt layer. The FIB cross-section obtained in the center of a contact ring of wafer A after 2000 h at 500°C is shown in Fig. 9b. After 2000 h at 500°C, the material contrast between the Pt and the TaSi$_x$ layers is not visible. The presence of voids in the upper and in the lower Pt layers suggests that significant migration of Pt into the TaSi$_x$ layer occurred. Also, the TaSi$_x$ layer shows a granular microstructure, which corresponds to the presence of grain-boundary diffusion paths. This behavior differs significantly from that of an ideal diffusion barrier. The thickness of the TaSi$_x$ layer increased from ~220 nm in the as-deposited state to about 390 nm after 2000 h at 500°C. This is believed to be caused by intermixing reactions.

In Fig. 10, a FIB cross-section of a Ti contact without the Ti/TaSi$_x$/Pt stack (wafer C) after 2000 h at 500°C is shown. The Ti contact layer and the

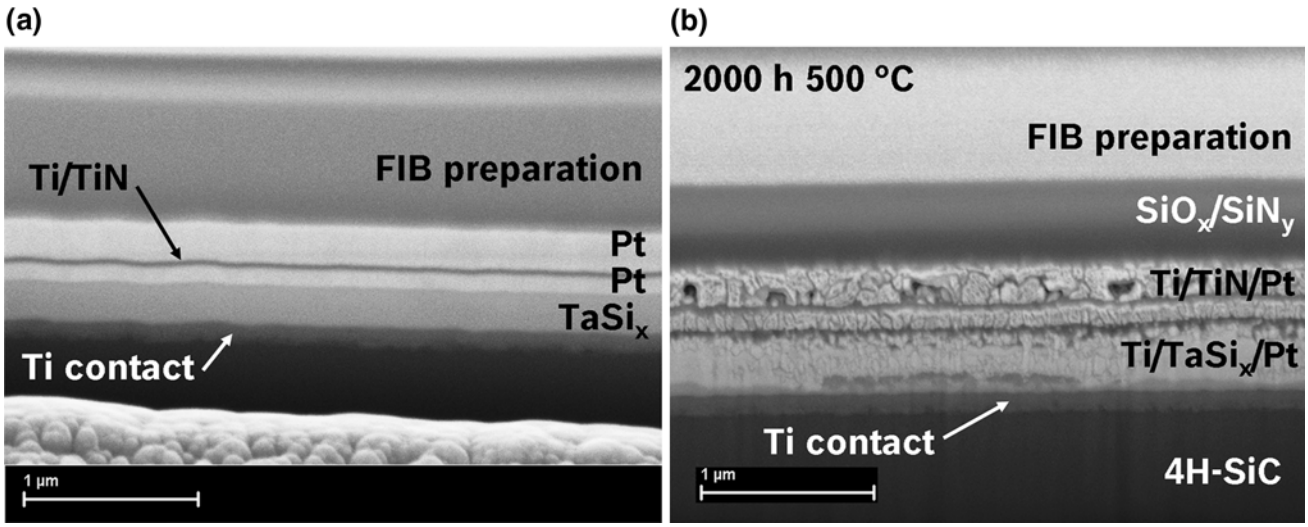

Fig. 9. SEM cross-sectional micrograph of a Ti contact (wafer A) after the deposition of the Ti/TaSi$_x$/Pt stack (a) and after aging for 2000 h at 500°C with the SiO$_x$/SiN$_y$ protective coating (b).

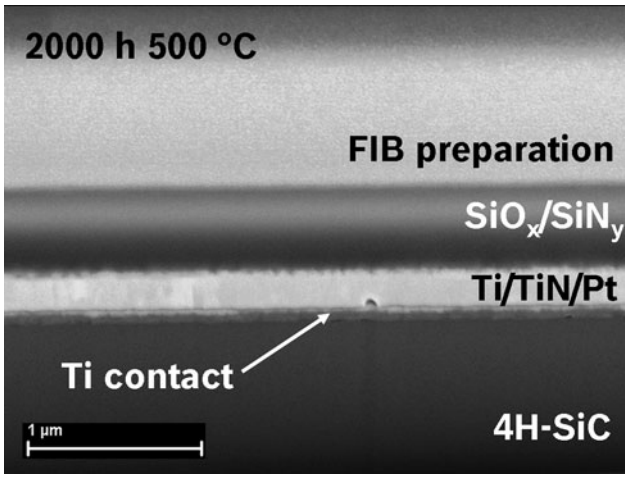

Fig. 10. SEM cross-sectional micrograph of a Ti contact without the Ti/TaSi$_x$/Pt stack (wafer C) after aging for 2000 h at 500°C.

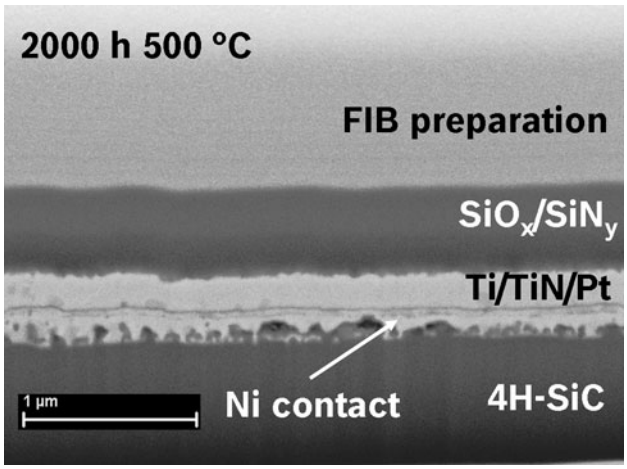

Fig. 11. SEM cross-sectional micrograph of a Ni contact without the Ti/TaSi$_x$/Pt stack (wafer D) after aging for 2000 h at 500°C.

Ti/TiN/Pt interconnect show a smooth topography, and no degradation of the contact metallization is visible in this cross-section. The corresponding cross-section of a Ni contact without the Ti/TaSi$_x$/Pt stack (wafer D) after 2000 h at 500°C is shown in Fig. 11. Here, a rough SiC/Ni contact interface as well as voids and an additional layer below the Ti/TiN/Pt interconnect are evident. These observations are consistent with detailed transmission electron microscopy (TEM) studies on as-processed Ni contacts to *n*-SiC,[20,24] where formation of Kirkendall voids at the SiC–contact interface and segregation of excess carbon to the top region of the contact layer were reported. The Ni contacts appear thus to be less stable than Ti contacts from the morphological point of view. Considering both the SEM cross-sectional analysis and the SCR data, it is evident that the Ti/TaSi$_x$/Pt diffusion barrier stack introduces a thermodynamic instability into the system, degrading its performance. Ti and Ni contacts without the Ti/TaSi$_x$/Pt stack exhibited excellent stability of the SCR, with the additional advantage of a simpler fabrication process.

CONCLUSIONS

In this work, we performed wafer-level measurements of the long-term stability of Ti and Ni ohmic contacts to *n*-4H-SiC during thermal treatments at 500°C in air and air/moisture environments. Statistical analysis of the specific contact resistance and of the contact failure ratio during the aging was carried out. SEM analysis and SEM cross-sectional analysis on samples prepared through the FIB technique were used to investigate the degradation mechanisms. We found that, through a stable protective coating, excellent stability of the contact metallization could be achieved, also when standard materials (sputtered Ti, TiN, and Pt) and thin films (total stack thickness <250 nm) were employed. In future work, further reliability testing and a more detailed material analysis necessary to understand the intermetallic reactions occurring in the contact metallizations during aging will be carried out.

REFERENCES

1. E. Kohn, *Comprehensive Microsystems*, Vol. 1 (Oxford: Elsevier Science, 2008), pp. 131–173.
2. R. Cheung, *Silicon Carbide Micro Electromechanical Systems for Harsh Environments* (London: Imperial College Press, 2006), pp. 128–168.
3. G.F. Eriksen and K. Dyrbye, *J. Micromech. Microeng.* 6, 55 (1996).
4. M.T. Soo, K.Y. Cheong, and A.F.M. Noor, *Sens. Actuators B* 151, 39 (2010).
5. R.S. Okojie, D. Spry, J. Krotine, C. Salupo, and D.R. Wheeler, *Mater. Res. Soc. Symp. Proc.*, Vol. 622 (2000), p. T8.3.1–6.
6. R.S. Okojie, D. Lukco, Y.L. Chen, and D.J. Spry, *J. Appl. Phys.* 91, 6553 (2002).
7. R.S. Okojie, D. Lukco, Y.L. Chen, D. Spry, and C. Salupo, *Mat. Res. Soc. Symp. Proc.* Vol. 640 (2001), p. H7.5.1–6.
8. A. Virshup, L.M. Porter, D. Lukco, K. Buchholt, L. Hultman, and A.L. Spetz, *J. Electron. Mater.* 38, 569 (2009).
9. S.-W. Lee, E.-K. Suh, N.-K. Cho, H.-D. Park, L. Uneus, and A.L. Spetz, *Solid State Electron.* 49, 1297 (2005).
10. R.M. Tiggelaar, R.G.P. Sanders, A.W. Groenland, and J.G.E. Gardeniers, *Sens. Actuators A* 152, 39 (2009).
11. S.L. Firebaugh, K.F. Jensen, and M.A. Schmidt, *J. Microelectromech. Syst.* 7, 128 (1998).
12. W.R. Farner, R. Job, and M. Werner, *Microsyst. Technol.* 7, 138 (2001).
13. W. Daves, A. Krauss, N. Behnel, V. Häublein, A. Bauer, and L. Frey, *Thin Solid Films* (2011). doi:10.1016/j.tsf.2011.02.089.
14. W. Daves, A. Krauss, M. Le-Huu, S. Kronmüller, V. Häublein, A. Bauer, and L. Frey, *Mater. Sci. Forum* 679–680, 449 (2011).
15. G.K. Reeves, *Solid State Electron.* 23, 487 (1980).
16. D.K. Schroder, *Semiconductor Material and Device Characterization* (Hoboken, NJ: Wiley, 2006), p. 127.
17. C.A. Hewett, M.J. Taylor, J.F. Zeidler, and M.W. Geis, *J. Appl. Phys.* 77, 755 (1995).
18. J.H. Park and P.H. Holloway, *J. Vac. Sci. Technol. B* 23, 2530 (2005).
19. M.H. Ervin, K.A. Jones, U. Lee, and M.C. Wood, *J. Vac. Sci. Technol. B* 24, 1185 (2006).
20. B. Pécz, *Appl. Surf. Sci.* 184, 287 (2001).

21. M. Siad, C.P. Vargas, M. Nkosi, D. Saidi, N. Souami, N. Daas, and A.C. Chami, *Appl. Surf. Sci.* 256, 256 (2009).
22. L.M. Porter and R.F. Davis, *Mater. Sci. Eng. B* 34, 83 (1995).
23. W.J. Choyke, H. Matsunami, and G. Pensl, *Silicon carbide. Recent major advances* (Heidelberg: Springer, 2004), pp. 343–366.
24. B. Pécz, *Phys. Stat. Sol.* 195, 214 (2003).